




One-pot synthesis, characterization, DNA binding and enzymatic studies of 4-methyl trans-cinnamate zinc(II)-mixed ligand complexes

Syeda Tahira Hafeez, Muhammad Nawaz Tahir, Saqib Ali, Muhammad Iqbal, Hussain Gulab & Khurram Shahzad Munawar

To cite this article: Syeda Tahira Hafeez, Muhammad Nawaz Tahir, Saqib Ali, Muhammad Iqbal, Hussain Gulab & Khurram Shahzad Munawar (2015) One-pot synthesis, characterization, DNA binding and enzymatic studies of 4-methyl trans-cinnamate zinc(II)-mixed ligand complexes, Journal of Coordination Chemistry, 68:20, 3636-3650, DOI: [10.1080/00958972.2015.1073269](https://doi.org/10.1080/00958972.2015.1073269)

To link to this article: <http://dx.doi.org/10.1080/00958972.2015.1073269>

 View supplementary material 

 Accepted author version posted online: 21 Jul 2015.
Published online: 12 Aug 2015.

 Submit your article to this journal 

 Article views: 99

 View related articles 

 View Crossmark data 

One-pot synthesis, characterization, DNA binding and enzymatic studies of 4-methyl *trans*-cinnamate zinc(II)-mixed ligand complexes

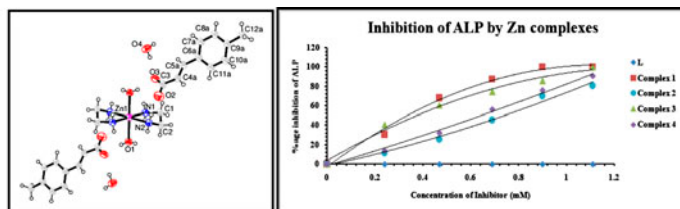
SYEDA TAHIRA HAFEEZ†, MUHAMMAD NAWAZ TAHIR‡, SAQIB ALI*†, MUHAMMAD IQBAL§, HUSSAIN GULAB§ and KHURRAM SHAHZAD MUNAWAR†

†Department of Chemistry, Quaid-i-Azam University, Islamabad, Pakistan

‡Department of Physics, University of Sargodha, Sargodha, Pakistan

§Department of Chemistry, Bacha Khan University, Charsadda, Pakistan

(Received 12 January 2015; accepted 7 July 2015)



Four new zinc(II) complexes formulated as $[\text{Zn}(\text{L})_2]$ (**1**), $[\text{Zn}(\text{L})_2(\text{phen})]$ (**2**), $[\text{Zn}(\text{L})_2(\text{bipy})\text{H}_2\text{O}]$ (**3**), and $[\text{Zn}(\text{en})_2(\text{H}_2\text{O})_2](\text{L})_2(\text{H}_2\text{O})_2$ (**4**), where HL = 4-methyl *trans*-cinnamic acid, bipy = 2,2'-bipyridine, phen = 1,10-phenanthroline, and en = ethylenediamine, have been synthesized and characterized by FT-IR and NMR spectroscopy. Single-crystal XRD revealed distorted square-pyramidal structure for **3** and octahedral for **4**. The complexes were screened for DNA interaction via vis-cometry and UV-visible spectroscopy. The apparent binding constants were calculated to be 1.18×10^4 , 1.26×10^5 , 4.64×10^4 , and 1.89×10^4 for **1–4**, respectively. The binding propensity to salmon sperm DNA was in the order: $K_2 > K_3 > K_4 > K_1$. Furthermore, these complexes demonstrated efficient inhibition of alkaline phosphatase, which was attributed to the binding of zinc(II) to the enzyme's active site.

Keywords: Zinc(II)-mixed ligand complexes; DNA binding; Alkaline phosphatase inhibition

1. Introduction

Carboxylate ligands have diverse coordination modes and give rise to a variety of complexes. The need for characterization of the metal enzyme centers and also exploration for new magnetic or catalytic materials causes an incessant interest in carboxylate chemistry [1]. Simple aromatic carboxylic acids (e.g. cinnamic acid) have biological applications and their binding with metals can have synergistic or antagonistic effect on biological activity [2]. Cinnamic

*Corresponding author. Email: drsa54@hotmail.com

acids and their derivatives are ubiquitous in plant species and possess pharmacological properties such as antioxidant, antidiabetic, and hepatoprotective [3]. They can scavenge free radicals and provide protection against certain kinds of mutagens and carcinogens [4].

It is of our interest to study the interaction of 4-methyl *trans*-cinnamic acid with zinc(II) and also to evaluate the effect of *N, N*-donor ligands on these complexes. Zinc is an essential and beneficial element for human growth. It regulates the activity of more than 300 metalloenzymes. Zinc also possesses antiviral, antibacterial, and wound-healing properties [2]. The relatively less explored zinc complexes can mimic active sites of the enzymes containing zinc and can serve as model complexes to study biological systems and have applications in supramolecular chemistry [5]. Zinc(II) ions are potent inhibitors of alkaline phosphatase (ALP), a hydrolase enzyme responsible for recycling of phosphates within the body. The inhibitory effect is due to the replacement of magnesium ions by zinc(II) on the enzyme's active site [6].

Design and synthesis of DNA-targeting complexes has significance and application in biotechnology, molecular biology, and medicine [7–9]. The interaction with DNA can be through covalent or non-covalent binding such as intercalation, groove, or electrostatic binding [7, 8, 10–12]. The nature of the metal center, ligands, co-ligands, or cofactors, pH, temperature, ionic strength, and reaction time are factors in the complex–DNA interactions. The understanding of such factors would help in designing new drugs [13, 14].

Mixed-ligand metal complexes of 2,2'-bipyridine (bipy), 1,10-phenanthroline (phen), or their modified variants can bind to DNA via a multitude of mechanisms and can cleave DNA duplex by virtue of their inherent chemical and photochemical reactivities [15]. Various analytical techniques can be used to study DNA interactions such as luminescence, fluorescence, viscosity measurements, UV–visible spectroscopy, and voltammetry [7, 10].

In the present study, we report synthesis and characterization of four new zinc(II)-mixed ligand complexes with oxygen- and nitrogen-donor ligands. Complexes **1–4** have been characterized by FT-IR and NMR spectroscopy. X-ray single-crystal structures for **2** and **4** are also reported. The interaction between salmon sperm DNA (SSDNA) and the complexes was investigated by UV–visible absorption spectroscopy and viscometry. The values of DNA-binding constant (K_b) and Gibb's free energy change have been calculated. The complexes were also screened for their ALP inhibition activity.

2. Experimental

2.1. Materials

$Zn(CH_3COO)_2 \cdot 2H_2O$, 4-methyl *trans*-cinnamic acid, 1,10-phenanthroline, 2,2'-bipyridine, ethylenediamine, Na_2CO_3 , $NaHCO_3$, and SSDNA were obtained from Fluka, Switzerland and used without purification. Methanol and DMSO were purchased from Merck, Germany and used without purification. Singly distilled water was used in the reactions. *p*-Nitrophenyl phosphate hexahydrate (*p*-NPP) was purchased from Sigma Aldrich, USA. ALP was extracted from human serum.

2.2. Physical measurements

The melting points were recorded on a Gallenkamp (UK) electrothermal melting point apparatus. IR spectra were recorded from 4000 to 400 cm^{-1} using a Thermo Nicolet-6700

(ATR) FT-IR spectrophotometer. ^1H and ^{13}C NMR spectra were recorded on a Bruker Avance Digital 300 MHz FT NMR spectrometer (Switzerland), at room temperature, using DMSO as an internal reference [δ ^1H (DMSO) = 2.5 and δ ^{13}C (DMSO) = 40 ppm]. Chemical shifts are given in ppm and coupling constant (J) values are in Hz. X-ray single crystal analyses data were collected on a Bruker Kappa APEX-II CCD diffractometer using graphite-monochromated Mo-K α radiation ($\lambda = 0.71073 \text{ \AA}$). The crystal structures were solved by direct methods followed by final refinement on F^2 with full-matrix least-squares using SHELXL-97 [16, 17]. DNA-binding studies by UV-visible spectroscopy and enzyme inhibition studies were performed on a UV-1601 Shimadzu spectrophotometer at room temperature ($25 \pm 1 \text{ }^\circ\text{C}$).

2.3. Procedure for the synthesis of 1–4

2.3.1. $[\text{Zn}(\text{L})_2]$ (1). Sodium bicarbonate (0.252 g, 3 mmol) was dissolved in distilled water (about 25 mL). An equimolar quantity of 4-methyl *trans*-cinnamic acid was added dropwise to the continuously stirring solution of sodium bicarbonate. The temperature of reaction mixture was adjusted to $50 \text{ }^\circ\text{C}$. After complete neutralization of acid with base, aqueous solution of zinc acetate dihydrate (0.329 g, 1.5 mmol) was added dropwise. The reaction mixture was stirred for another 2–3 h under the same conditions. The final product was filtered, washed with distilled water, and air dried (figure 1).

Color and state: white powder; Yield: 0.64 g (79%); m.p.: $365\text{--}366 \text{ }^\circ\text{C}$; FT-IR (cm^{-1}): $1507 \nu(\text{OCO})_{\text{asym}}$, $1380 \nu(\text{OCO})_{\text{sym}}$, $\Delta\nu = 127$, $1638 \nu(\text{C}=\text{C})$, $3022 \nu(\text{Ar-H})$, $2914 \nu(\text{CH}_3)$, $420 \nu(\text{Zn-O})$.

2.3.2. $[\text{Zn}(\text{L})_2\text{phen}]$ (2). The sodium salt of 4-methyl *trans*-cinnamic acid (NaL) was prepared by the same method as that for 1. After addition of zinc acetate dihydrate

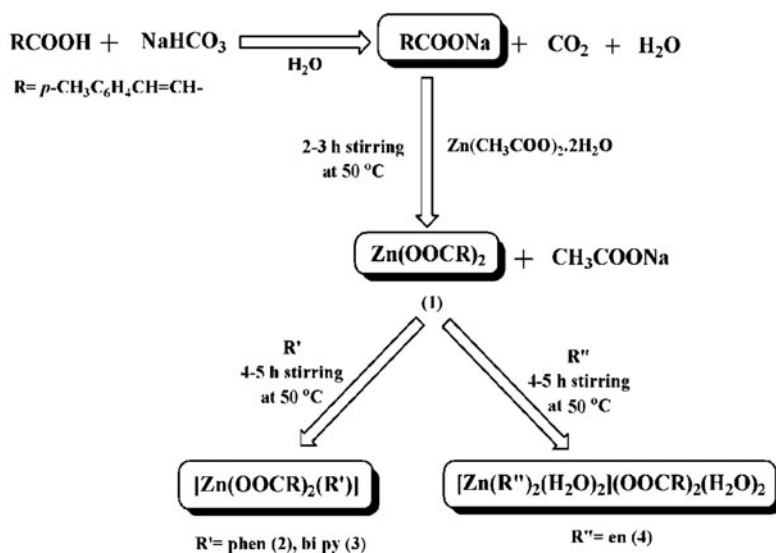


Figure 1. Scheme for synthesis of 1–4.

(0.329 g, 1.5 mmol) followed by 2–3 h stirring, 1,10-phenanthroline (0.297 g, 1.5 mM) was added. Stirring was continued for another 4–5 h under the same conditions. The final product was filtered, washed with distilled water, and air dried (figure 1).

Color and state: white powder; Yield: 0.78 g (70%); m.p.: 341–342 °C; FT-IR (cm)⁻¹: 1507 $\nu(\text{OCO})_{\text{asym}}$, 1354 $\nu(\text{OCO})_{\text{sym}}$, $\Delta\nu = 153$, 1641 $\nu(\text{C}=\text{C})$, 3066 $\nu(\text{Ar}-\text{H})$, 2922 $\nu(\text{CH}_3)$, 521 $\nu(\text{Zn}-\text{N})$, 418 $\nu(\text{Zn}-\text{O})$.

2.3.3. [Zn(L)₂(bipy)H₂O] (3). Complex 3 was prepared by same procedure as 2, except 2,2'-bipyridine (0.234 g, 1.5 mM) was used as co-ligand instead of 1,10-phenanthroline in the final step (figure 1). The final product was crystallized in methanol.

Color and state: white crystalline; Yield: 0.75 g (72%); m.p.: 319–320 °C; FT-IR (cm)⁻¹: 1575 $\nu(\text{OCO})_{\text{asym}}$, 1372 $\nu(\text{OCO})_{\text{sym}}$, $\Delta\nu = 203$, 1636 $\nu(\text{C}=\text{C})$, 3031 $\nu(\text{Ar}-\text{H})$, 2925 $\nu(\text{CH}_3)$, 524 $\nu(\text{Zn}-\text{N})$, 421 $\nu(\text{Zn}-\text{O})$.

2.3.4. [Zn(en)₂(H₂O)₂](L)₂(H₂O)₂ (4). Complex 4 was also prepared by same method as 2 and 3, with ethylenediamine added as co-ligand in the final step (figure 1). For 4, the product was soluble in water which was rotary evaporated. The solid residue was washed with methanol and recrystallized in distilled water.

Color and state: white crystalline; Yield: 0.74 g (75%); m.p.: 149–150 °C; FT-IR (cm)⁻¹: 1561 $\nu(\text{OCO})_{\text{asym}}$, 1385 $\nu(\text{OCO})_{\text{sym}}$, $\Delta\nu = 176$, 1640 $\nu(\text{C}=\text{C})$, 3031 $\nu(\text{Ar}-\text{H})$, 2920 $\nu(\text{CH}_3)$, 537 $\nu(\text{Zn}-\text{N})$, 431 $\nu(\text{Zn}-\text{O})$.

2.4. DNA interaction studies by viscosity measurements

Ubbelohde viscometer was used to perform viscometric measurements. Experiments were performed at 25 ± 1 °C and flow time was measured using a digital stop watch. The average of triplicate measurements was taken for each measurement. Between the successive measurements, the viscometer was rinsed with acetone and air dried. Data are presented as plots of relative viscosity $(\eta/\eta^0)^{1/3}$, versus compound-DNA ratio [(Compound)/(DNA)], where η and η^0 are DNA viscosities, in the presence and absence of the complex, respectively [18, 19].

2.5. DNA interaction studies by UV-visible spectroscopy

Solution of commercial SSDNA was prepared in distilled water and kept at 4 °C. From the absorbance at 260 and 280 nm (A_{260}/A_{280}), nucleotide to protein (N/P) ratio was greater than 1.8, which indicated that the DNA was free from protein. The SSDNA concentration was calculated via absorption spectroscopy using the molar absorption coefficient (ϵ) value of 6600 M⁻¹ cm⁻¹ (260 nm) for DNA [20–23] and was found to be 4.75 × 10⁻⁵ M. This stock solution was used to prepare working solutions by dilution. Both the sample and the SSDNA solution were prepared in 50% aqueous DMSO.

During the UV absorbance titrations, the concentration of the compound (0.25 mM) was kept constant, while that of DNA was varied. To the sample and the reference solutions, an equivalent concentration of DNA was added to correct for the absorbance of DNA. Before the absorbance measurements, compound-DNA solutions were allowed to equilibrate for

10 min. Absorbance spectra were recorded using a UV-1601 Shimadzu spectrophotometer at 25 ± 1 °C.

2.6. Assay of ALP activity

The inhibition of ALP was assayed by monitoring the rate of hydrolysis of *p*-nitrophenyl phosphate (*p*NPP) at 25 °C. The assays were prepared using the same method as reported earlier by our research group [24–27] with slight modifications. The working substrate solution was prepared by mixing four parts of reagent A (diethanolamine pH 9.8, 2 mol dm⁻³ and magnesium chloride 0.5 mmol dm⁻³) and one part of reagent B (*p*-nitrophenyl phosphate 50 mmol dm⁻³). The substrate solution was incubated for 5 m at 25 °C. Two milliliters of the substrate was taken in a cuvette and 40 μL of human serum having an activity of 165 IU L⁻¹ was added. After incubation for 1 min, the absorbance was measured to check the activity of the enzyme. ALP hydrolyzed the *p*-NPP and yellow-colored *p*-nitrophenol was produced as shown in figure 2.

Varying concentrations of solutions of 1–4 (20, 40, 60, and 80 μL) from a 12.5 mM stock solution were added periodically into the cuvette and the mixtures were further incubated for 3 min. The release of the yellow-colored *p*-NPP chromophore was monitored at $\lambda = 405$ nm. For accurate results, absorbance measurements were recorded per minute up to 5 min, and the average value of this period was used, from which the % inhibition was calculated.

3. Results and discussion

3.1. FT-IR data

The frequencies of interest are those associated with the carboxylate group, Zn–O and Zn–N. The asymmetric and symmetric vibrations for the COO group appeared at 1507 and 1380, 1507 and 1354, 1575 and 1372, 1561, and 1385 cm⁻¹ for 1–4, respectively. The difference between the two vibration modes, i.e. $\Delta\nu$ is used as a spectroscopic criterion to predict binding mode of the carboxylate moiety with the metal center [28]. The peak position of asymmetric and symmetric vibrations for COO is sensitive to electronic charge density of C–O bond; higher the difference in their electronic charge density, higher will be the value of asymmetric vibration and lower will be that of symmetric vibration [4].

The broadbands observed for 3 and 4 from 2550 to 3600 cm⁻¹ correspond to the O–H of water. The C–H stretching vibrations for the aromatic moiety were observed at 3022, 3066, 3031, and 3031 cm⁻¹ for 1–4, respectively. The band at 2914–2925 cm⁻¹ for 1–4

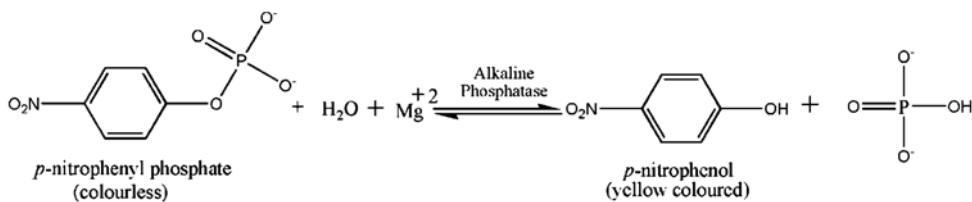


Figure 2. Hydrolysis of *p*-nitrophenyl phosphate by ALP.

corresponds to C–H bond of the methyl. The vibration bands at 1638, 1641, 1636, and 1640 cm^{-1} correspond to $-\text{C}=\text{C}-$ present in conjugation with the aromatic moiety. For **2–4**, bands corresponding to Zn–N vibration appeared at 521, 524, and 537 cm^{-1} , respectively. The absorption band corresponding to Zn–O bond stretching was observed in the range of 420, 418, 421, and 431 cm^{-1} for **1–4**, respectively.

3.2. NMR data

^1H NMR and ^{13}C NMR chemical shifts of HL and its complexes are given in table 1 (atom numbering is given in figure 3), where comparative NMR analysis shows complex formation. In NaL, O–H signal (at 12.38 ppm) of HL disappeared. In ^1H NMR of all four complexes, signals owing to olefinic protons are from 6.41 to 7.42 ppm, and one signal of methyl proton is obtained at 2.30–2.35 ppm. Two signals for **1** and **4**, while six signals for **2** and **3** appeared in the aromatic region. These additional four signals (for **2** at 9.18 (d), 8.10 and 8.13 ppm (dd), 8.88 and 8.90 (dd), 8.25 ppm (s) and for **3** at 8.81 (d), 7.72 (m), 8.21 (m) and 8.61 ppm (d)) correspond to 1,10-phenanthroline and 2,2'-bipyridine, respectively. In **4**, two singlets corresponding to the ethylenediamine (at 1.93 ppm (s) for NH_2 and at 2.78 ppm (s) for CH_2) also appeared along with the signals belonging to carboxylate. For **3** and **4**, singlets at 3.39 and 3.35 ppm gave evidence of coordinated water.

The ^{13}C NMR data of HL was also compared with its Zn(II) complexes. In the ligand spectrum, signal at 168.16 ppm was assigned to carboxylate carbon C^1 . The peak position is sensitive to change in its environment and is indicative of complexation. Signal for C^1 appeared at 168.16 ppm for HL and at 172.69, 173.30, and 171.33 ppm for **1**, **3**, and **4**, respectively. When the carboxylate moiety binds bidentate to the metal center, C^1 gets deshielded. In our complexes, C^1 undergoes deshielding of 3–5 ppm. This may be due to monodentate binding of 4-methyl *trans*-cinnamate to zinc. The observation was further strengthened by crystal structures of **3** and **4**. Signals for bipy appeared at 149.59, 120.74, 140.23, 126.54, and 149.13 ppm for **3**. In **4**, signal for CH_2 of ethylenediamine appeared at 24.72 ppm.

Table 1. ^1H and ^{13}C NMR data (ppm) of zinc(II) complexes with 4-methyl *trans*-cinnamic acid (HL).

$^1\text{H}/^{13}\text{C}$	4-methyl <i>trans</i> -cinnamic acid (HL)	NaL	1	2	3	4
O–H	12.38 (s)	–	–	–	–	–
H^2	7.21 (d) [15.90]	7.21 (d) [16.20]	7.37 (d) [15.90]	7.42 (d) [15.90]	7.35 (d) [15.90]	7.39 (d) [16.20]
H^3	6.47 (d) [16.20]	6.31 (d) [15.90]	6.48 (d) [15.90]	6.41 (d) [15.90]	6.44 (d) [15.90]	6.47 (d) [15.90]
$\text{H}^{5,5\Sigma}$	7.56 (d) [7.50]	7.11 (d) [7.80]	7.20 (d) [7.50]	7.22 (d) [7.50]	7.17 (d) [7.50]	7.19 (d) [8.10]
$\text{H}^{6, 6\Sigma}$	7.60 (d) [7.50]	7.339 (d) [8.10]	7.49 (d) [7.50]	7.47 (d) [7.50]	7.46 (d) [7.50]	7.42 (d) [8.10]
H^8	2.31 (s)	2.197 (s)	2.31 (s)	2.32 (s)	2.30 (s)	2.35 (s)
C^1	168.16	175.88	172.69	–	173.30	171.33
C^2	144.40	140.77	140.94	–	141.01	139.89
C^3	140.61	140.23	139.32	–	139.31	138.18
C^4	118.54	122.94	123.13	–	123.03	122.95
$\text{C}^{5,5\Sigma}$	128.66	127.64	128.04	–	128.01	127.49
$\text{C}^{6, 6\Sigma}$	129.97	129.49	129.86	–	129.84	129.73
C^7	131.95	132.20	132.98	–	132.96	133.98
C^8	21.47	20.36	21.40	–	21.39	21.33

Note: Values in square brackets show the [$^1\text{H}, ^1\text{H}$] coupling in Hz.

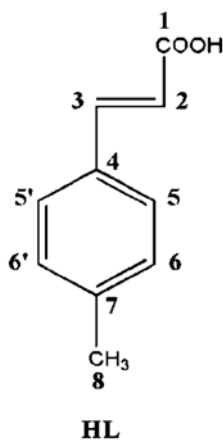


Figure 3. Numbering scheme of HL for ^1H and ^{13}C NMR interpretation.

3.3. Single crystal X-ray analysis

Crystallographic data and summary of the refinement parameters for the complexes are given in table 2.

3.3.1. Crystal structure of 3. Crystal structure for 3 along with the atom connectivities is shown in figure 4. The crystal was refined in the monoclinic crystal system with space group

Table 2. Crystal data and refinement parameters for 3 and 4.

Complex	3	4
Chemical formula	$\text{C}_{30}\text{H}_{28}\text{N}_2\text{O}_5\text{Zn}$	$\text{C}_{24}\text{H}_{42}\text{N}_4\text{O}_8\text{Zn}$
Formula weight	561.910	579.99
T (K)	296(2)	296(2)
Wavelength (\AA)	0.71073	0.71073
Crystal system	Monoclinic	Monoclinic
Space group	Pn	$P2_1/n$
a (\AA)	5.6114(7)	7.6168(5)
b (\AA)	8.1426(10)	6.0296(3)
c (\AA)	28.490(3)	30.9371(19)
α ($^\circ$)	90	90
β ($^\circ$)	95.023(9)	96.142(3)
γ ($^\circ$)	90	90
V (\AA^3)	1296.8(3)	1412.67(15)
Z	2	2
Absorption coefficient (mm^{-1})	0.991	0.921
$F(0\ 0\ 0)$	584	616
Crystal size (mm)	$0.35 \times 0.20 \times 0.18$	$0.35 \times 0.28 \times 0.25$
θ range for data calculation	1.43–26.00	2.65–26.00
Reflection collected	4856	2773
Independent reflection	3417	2307
Goodness-of-fit on F^2	1.018	1.031
Final R indices [$I > 2\sigma(I)$]	$R_1 = 0.0623$ $wR_2 = 0.1137$	$R_1 = 0.0387$ $wR_2 = 0.0896$
R indices (all data)	$R_1 = 0.0942$ $wR_2 = 0.1262$	$R_1 = 0.0495$ $wR_2 = 0.0950$
Data/restraints/parameters	4856/4/350	2773/6/133

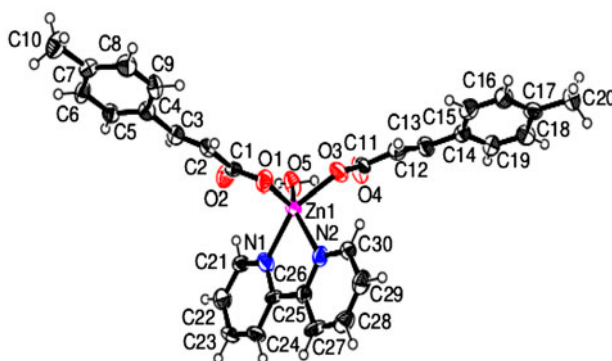


Figure 4. ORTEP drawing with the numbering scheme of **3** (thermal ellipsoids are drawn at 50% probability level).

Pn. The molecular structure of **3** revealed that in the complex, zinc is five coordinated, bonded to two oxygens of two carboxylate ligands, two nitrogens of bipy, and a water molecule. Both carboxylates show monodentate coordination, while bipy is bidentate. The crystal data are given in table 2, while selected bond lengths and angles are given in table 3.

The geometry around zinc can be characterized by τ (Σ) value, i.e. structural distortion index, $\Sigma = (\beta - \alpha)/60$, where $1/\beta$ corresponds to the largest and α to the second largest basal angle around zinc. For **3**, it was calculated to be 0.21. For the perfect square-pyramidal geometry, Σ is zero ($\alpha = \beta = 180^\circ$), and for the perfect trigonal-bipyramidal geometry, it is unity ($\alpha = 120^\circ$) [29, 30]. The calculated Σ value of 0.21 for the complex suggests a distorted square-pyramidal arrangement around zinc(II).

The two carboxylate groups chelate to zinc in an asymmetric manner, which is reflected by a shorter Zn–O1 [1.992(5) Å] bond and a longer Zn–O3 [2.055(5) Å] bond. The asymmetric coordination is further confirmed by an unequal O–C bond distance. The shorter Zn–O1 bond is accompanied by a longer O1–C1 bond distance [1.294(8) Å] and the longer Zn–O3 is accompanied by a shorter O3–C11 bond distance [1.268(9) Å]. The steric hindrance induced by the bulky carboxylate ligands, electron pair repulsion and the presence of bipyridine may be responsible for this discrepancy.

The Zn–O_{H₂O} bond length is 2.054(6) Å. The nitrogens of bipy also have asymmetric bond distances; Zn–N1 [2.122(7) Å] and Zn–N2 [2.180(7) Å].

The water molecule in the structure is responsible for intramolecular as well as intermolecular H-bonding; bipyridine rings also undergo intermolecular H-bonding as evident from the packing diagram shown in figure 5. The molecules form 1-D polymeric chains with base vector [1 0 0].

3.3.2. Crystal structure of 4. The crystal structure of **4** is depicted in figure 6. Selected bond lengths and angles for **4** are given in table 3, while crystallographic parameters are given in table 2. In this complex, zinc(II) is coordinated with two ethylenediamine groups and two water molecules. All six bonds around zinc are coordinate covalent type. The geometry around zinc is octahedral and the space group is *P* 2₁/*n* with monoclinic crystal system. The bond distances around zinc are almost symmetric for ethylenediamine and same is the case for both water molecules.

Table 3. Selected bond lengths (Å) and angles (°) of **3** and **4**.

Complex	3	4
Bond lengths (Å)		
Zn–O1	1.992(5)	2.2574(17)
Zn–O3	2.055(5)	—
Zn–O5	2.054(6)	—
Zn–N1	2.122(7)	2.136(2)
Zn–N2	2.180(7)	2.1379(19)
N1–C1	—	1.472(3)
N2–C2	—	1.468(2)
O1–C1	1.294(8)	—
O2–C1	1.206(10)	—
O2–C3	—	1.2352(17)
O3–C3	—	1.2630(15)
O3–C11	1.268(9)	—
O4–C11	1.218(11)	—
Bond angles (°)		
O1–Zn–O1	—	180.00
O1–Zn–O3	96.1(2)	—
O1–Zn–O5	120.3(2)	—
O3–Zn–O5	86.1(2)	—
O1–Zn–N1	105.2(2)	89.67(7)
O1–Zn–N2	97.8(2)	92.58(7)
O3–Zn–N1	154.3(2)	—
O3–Zn–N2	86.7(2)	—
O5–Zn–N1	95.2(3)	—
O5–Zn–N2	141.7(3)	—
N1–Zn–N2	76.4(3)	98.32(7)
N1–Zn–N1	—	180.00
N2–Zn–N2	—	180.00
C1–N1–Zn	—	108.54(15)
C2–N2–Zn	—	107.31(12)
Zn–O1–C1	109.9(5)	—
Zn–O3–C11	127.8(5)	—
N1–C1–C2	—	109.8(2)
N2–C2–C1	—	108.95(13)
O2–C3–O3	—	123.62(11)

In **4**, zinc carries +2 charge, which is balanced by carboxylate ligands present outside the coordination sphere. There are also two water molecules present outside the coordination sphere. Figure 7 shows packing diagram of **4**. The molecules form a 2-D polymeric network with base vector [1 0 0], [0 1 0], and in the plane (0 0 1).

3.4. DNA-binding studies by UV-visible spectroscopy

The interaction of the synthesized complexes with DNA was studied by electronic absorption spectroscopy. The effect of increasing concentration of SSDNA on the complex was studied by comparing absorbance of the free complex (0.25 mM) and the complex–DNA adduct. The absorbance titration experiments were performed by keeping the concentration of complex constant and varying DNA concentration (2.26–13.57 μM). Successive addition of DNA produces change in electronic absorption spectrum of the complex, indicating interaction of the complex with DNA.

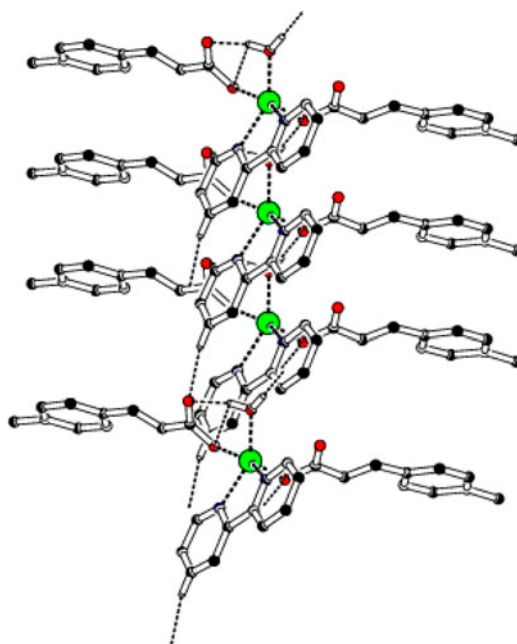


Figure 5. Packing diagram of **3** (hydrogens not involved in H-bonding are omitted for clarity).

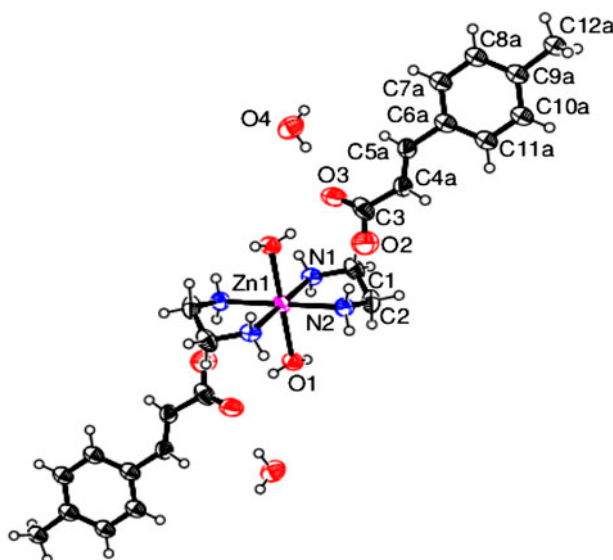


Figure 6. ORTEP drawing with the numbering scheme of **4** (thermal ellipsoids are drawn at 50% probability level).

Benesi–Hildebrand equation [equation (1)] [7, 8] was employed to evaluate binding parameters:

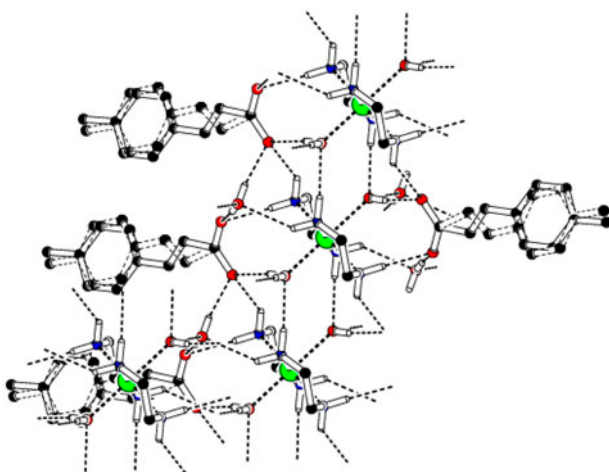


Figure 7. Packing diagram of **4** (hydrogens not involved in H-bonding are omitted for clarity).

$$\frac{A_o}{A - A_o} = \frac{\varepsilon_G}{\varepsilon_{H-G} - \varepsilon_G} + \frac{\varepsilon_G}{\varepsilon_{H-G} - \varepsilon_G} \cdot \frac{1}{K[\text{DNA}]} \quad (1)$$

where K is binding constant, A and A_o are absorbances of the complex–DNA adduct and pure complex, ε_{H-G} , and ε_G are molar absorption coefficients of the complex–DNA adduct and complex, respectively. Association/binding constants were calculated from the intercept-to-slope ratio of the plot of $1/[\text{DNA}]$ along the abscissa and $A_o/A - A_o$ along the ordinate [31]. The change in Gibb's free energy was calculated using the following equation [7, 8]:

$$\Delta G = -RT \ln (K) \quad (2)$$

Figure 8 depicts the absorption spectrum of **1** along with plots of $A_o/(A - A_o)$ versus $1/[\text{DNA}]$ for **1–4**, respectively. The best fit line, superimposed on the data according to equation (1) yields DNA-binding constants (K) and Gibb's free energy change (ΔG) of the complex–SSDNA adduct. (The UV–visible spectra of 0.25 mM **2–4** can be seen in figure S1 (see online supplemental material at <http://dx.doi.org/10.1080/00958972.2015.1073269>), and data for the plots B–D, in tables S1–S4 of Supplementary materials). The calculated values of binding constants and Gibb's free energy change (ΔG) for **1–4** are given in table 4.

Absorbance spectra of the four complexes exhibit a single broadband with λ_{max} at 272.4, 279.0, 275.2, and 274.4 nm for **1–4**, respectively. The band corresponds to the $\pi-\pi^*$ transitions of ligand-based aromatic moiety. The strong absorbance of these compounds in the near-UV region (272–295 nm) is attributed to the long-living triplet excited state of the aromatic system [8].

Incremental addition of DNA lowers the intensity of absorbance, i.e. hypochromic effect with no prominent red shift in λ_{max} . The hypochromism may be due to either compactness in the structure of the complex alone or in the complex–DNA adduct. Hypochromic effect with no prominent shift ($\Delta\lambda \leq 8$ nm) indicates outside binding (groove binding) as a dominant mode of interaction [32]. Groove binders induce little or no structural rearrangement in the DNA and show binding propensity for the AT-rich DNA pockets. The AT-rich base

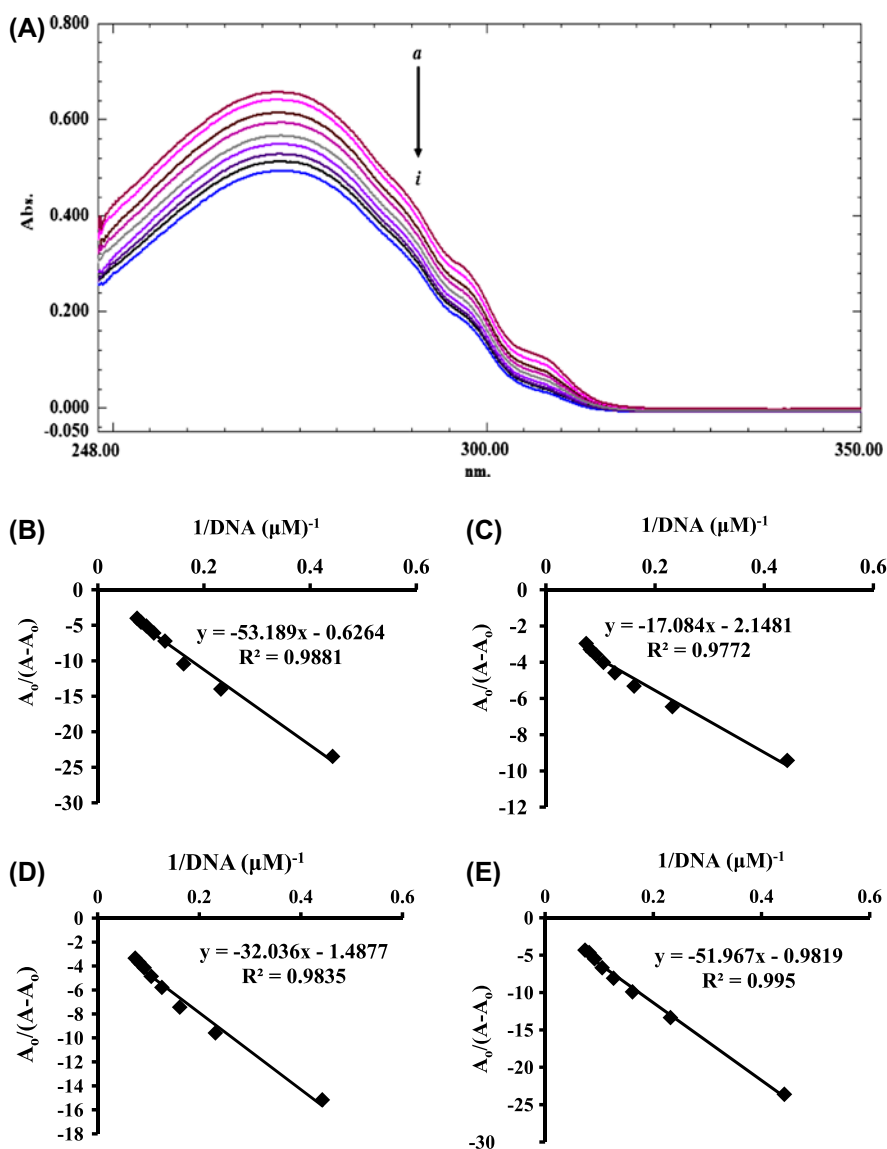


Figure 8. (A) Absorption spectra of 0.25 mM **1** in the absence (a) and presence of 2.26 (b), 4.32 (c), 6.20 (d), 7.92 (e), 9.50 (f), 10.96 (g), 12.32 (h), and 13.57 (i) μM SSDNA. The arrow direction indicates the increasing SSDNA concentration. (B–D) Plots of $A_0/(A - A_0)$ vs. $1/[\text{DNA}]$ for **1–4**, respectively. The best fit line, superimposed on the data according to equation (1) yielded DNA-binding constants (K) and Gibbs's free energy change (ΔG) of the complex–SSDNA adduct.

pairs not only possess H-bond acceptors (N3 of adenine and O2 of thymine), but can also develop favorable hydrophobic interactions between the adenine C2 hydrogens and the aromatic rings present in the DNA-binding complexes [20, 33]. The low affinity DNA binders have $K_b < 10^5$ [34], so among the synthesized complexes, **2** is a strong binder, while **1**, **3**, and **4** are weak binders. Highest binding affinity of **2** can be attributed to its extended aromatic moiety [35]. Overall, the calculated intrinsic binding constants for **1–4** are in

Table 4. UV-visible and DNA-binding data for **1–4**.

Complex	λ_{\max} (nm)	K (M^{-1})	ΔG (kJ mol^{-1})
1	272.4	1.18×10^4	-23.22
2	279.0	1.26×10^5	-29.09
3	275.2	4.64×10^4	-26.62
4	274.4	1.89×10^4	-24.39

agreement with those previously reported for Zn(II) complexes [34]. The negative value of ΔG is indicative of the spontaneity of the complex–DNA adduct formation.

3.5. Viscosity measurements

The viscosity measurements are an effective tool while studying the interaction of small molecules with DNA. The viscosity of DNA solution is sensitive to the variation in length of DNA. Therefore, measurement of DNA viscosity is considered as a critical method for elucidation of the complex–DNA interaction mode. Measurement of relative viscosity has proved to be a reliable technique for DNA-binding studies. When a complex exclusively binds in the DNA grooves, it causes a kink or bend in DNA helix thus reducing its effective length which results in a decrease in the DNA solution's viscosity [8, 19, 36].

A series of solutions were made keeping DNA concentration constant (4.75×10^{-5} M), and concentrations of **1–4** were varied. All of the samples were allowed to equilibrate for 10 min prior to the flow time measurement. The values of the relative viscosity $(\eta/\eta_0)^{1/3}$ were calculated from $(t/t_0)^{1/3}$ ratio for all the samples, where η , η_0 , t , and t_0 represent the viscosity and time of the DNA solution in the presence and the absence of the complex, respectively. Plot of $(\eta/\eta_0)^{1/3}$ versus (compound)/(DNA) ratio is shown in figure 9, indicating that the viscosity decreases upon addition of increasing the amount of compound in each case, therefore, the groove-binding mode is deduced as binding mode of the complexes with DNA. The predicted mode is in agreement with the results of UV-visible spectroscopy.

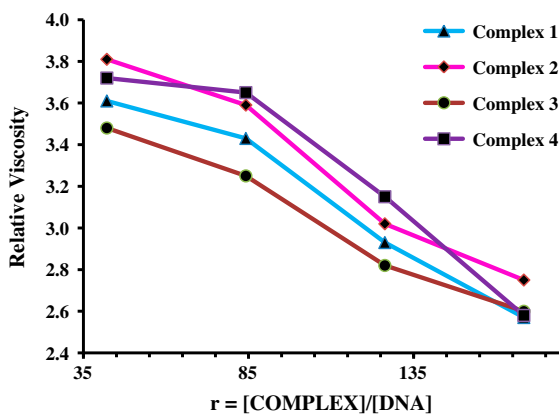


Figure 9. Effect of increasing concentration of **1–4** on relative viscosity of SSDNA.

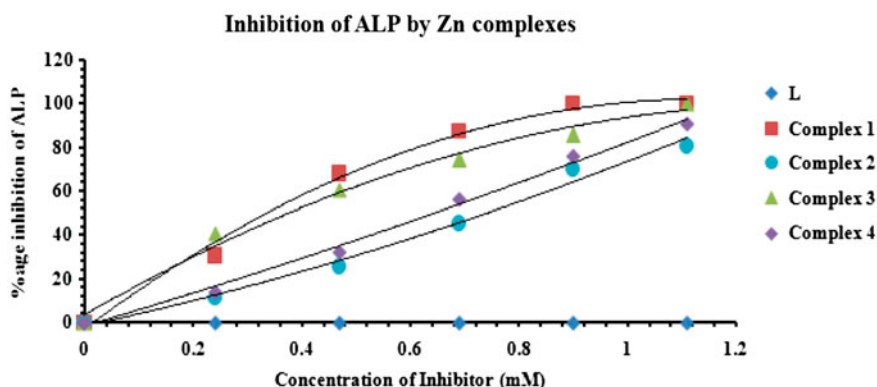


Figure 10. ALP inhibition profile of ligand and its Zn(II) complexes (1–4).

3.6. ALP inhibition study

The effect of varying concentration of synthesized zinc(II) complexes on the activity of the enzyme; ALP was studied for hydrolysis of *p*-NPP (*p*-nitrophenylphosphate). ALP catalyzes the transfer of phosphate groups to alcohol (transphosphorylation) or water (hydrolysis) using a variety of phosphor-monoesters and are characterized by a high-pH optima and a broad range of substrate specificity [37]. The concentration of *p*-NPP is directly related to the activity of inhibitor and was monitored spectrophotometrically. Here, we have observed that the ligand itself was inactive against ALP. For 1–4, observed maximum values of % inhibition were 100, 80.6, 100, and 90.54, respectively, at 1.11 mM concentration (figure 10). A comparison of inhibition activities of ligand and its complexes indicates that these might be the Zn²⁺ responsible for deactivation of enzyme. Zinc ions decrease enzyme's activity by occupying Mg²⁺-binding sites, in addition to Zn²⁺-binding sites, thus rendering the enzyme's active sites blocked [6].

4. Conclusion

Four new zinc(II) complexes of 4-methyl *trans*-cinnamate as a main ligand and 1,10-phenanthroline, 2,2'-bipyridine, and ethylenediamine as co-ligands have been synthesized and characterized by FT-IR and NMR spectroscopy. Distorted square-pyramidal structure for 3 and octahedral for 4 were confirmed by single-crystal XRD. DNA-binding studies by UV-visible spectroscopy and viscometry illustrated groove-binding mode of the complexes with SSDNA. Negative ΔG values indicate spontaneity of binding with SSDNA. ALP inhibition studies revealed that the complexes are inhibitors of ALP and inhibition is concentration dependant.

Supplementary material

Crystallographic data for the crystal structures reported in this article have been deposited with the Cambridge Crystallographic Data Center, CCDC # 1042909 (3) and 1042910 (4). Copies of this information may be obtained free of charge from the Director, CCDC, 12 Union Road, Cambridge CB2 1EZ [Fax: +44(1223)336-033 or Email: deposit@ccdc.cam.ac.uk].

Disclosure statement

No potential conflict of interest was reported by the authors.

References

- [1] D. Dobrzyńska, T. Lis, L.B. Jerzykiewicz. *Inorg. Chem. Commun.*, **8**, 1090 (2005).
- [2] V. Zelenák, M. Sabo, W. Massa, P. Llewellyn. *Inorg. Chim. Acta*, **357**, 2049 (2004).
- [3] S. Adisakwattana, W. Sompong, A. Meepprom, S. Ngamukote, S. Yibchok-anun. *Int. J. Mol. Sci.*, **13**, 1778 (2012).
- [4] V. Zelenák, I. Císařová, P. Llewellyn. *Inorg. Chem. Commun.*, **10**, 27 (2007).
- [5] S. Caglar, S. Demir, Z. Heren, O. Büyükgüngör. *Polyhedron*, **30**, 1389 (2011).
- [6] R.L. Dean. *Biochem. Mol. Biol. Educ.*, **30**, 401 (2002).
- [7] M. Sirajuddin, S. Ali, N.A. Shah, M.R. Khan, M.N. Tahir, , *Spectrochim. Acta, Part A*, **94**, 134 (2012).
- [8] M. Sirajuddin, S. Ali, A. Haider, N.A. Shah, A. Shah, M.R. Khan. *Polyhedron*, **40**, 19 (2012).
- [9] Y.-G. Sun, K.-L. Li, Z.-H. Xu, T.-Y. Lv, S.-J. Wang, L.-X. You, F. Ding. *J. Coord. Chem.*, **66**, 2455 (2013).
- [10] F. Asghar, A. Badshah, A. Shah, M.K. Rauf, M.I. Ali, M.N. Tahir, E. Nosheen, Z. Rehman, R. Qureshi. *J. Organomet. Chem.*, **717**, 1 (2012).
- [11] M. Jiang, Y.-T. Li, Z.-Y. Wu. *J. Coord. Chem.*, **65**, 1858 (2012).
- [12] H. Wu, Y. Bai, J. Yuan, H. Wang, G. Pan, X. Fan, J. Kong. *J. Coord. Chem.*, **65**, 2839 (2012).
- [13] D.-D. Li, Z.-W. Tao. *J. Coord. Chem.*, **66**, 4237 (2013).
- [14] K. Pothiraj, T. Baskaran, N. Raman. *J. Coord. Chem.*, **65**, 2110 (2012).
- [15] C.V. Sastri, D. Eswaramoorthy, L. Giribabu, B.G. Maiya. *J. Inorg. Biochem.*, **94**, 138 (2003).
- [16] G.M. Sheldrick. *SHELXS-97, Program for X-ray Crystal Structure Solution*, Göttingen University, Göttingen (1997).
- [17] G.M. Sheldrick. *SHELXS-97, Program for X-ray Crystal Structure Refinement*, Göttingen University, Göttingen (1997).
- [18] J. Liu, T. Zhang, T. Lu, L. Qu, H. Zhou, Q. Zhang, L. Ji. *J. Inorg. Biochem.*, **91**, 269 (2002).
- [19] J. Lu, H. Guo, Y. Zhang, J. Jiang, Y. Liu, L. Zang, J. Huang. *J. Coord. Chem.*, **65**, 1765 (2012).
- [20] M. Sirajuddin, S. Ali, A. Badshah. *J. Photochem. Photobiol., B*, **124**, 1 (2013).
- [21] R.A. Hussain, A. Badshah, M.N. Tahir, B. Lal, I.A. Khan. *Aust. J. Chem.*, **66**, 626 (2013).
- [22] A.K. Asatkar, S. Nair, V.K. Verma, C.S. Verma, T.A. Jain, R. Singh, S.K. Gupta, R.J. Butcher. *J. Coord. Chem.*, **65**, 28 (2012).
- [23] Y.-F. Chen, M. Liu, J.-W. Mao, H.-T. Song, H. Zhou, Z.-Q. Pan. *J. Coord. Chem.*, **65**, 3413 (2012).
- [24] T. Koike, E. Kimura. *J. Am. Chem. Soc.*, **113**, 8935 (1991).
- [25] W.H. Chapman Jr., R. Breslow. *J. Am. Chem. Soc.*, **117**, 5462 (1995).
- [26] S.T. Hafeez, S. Ali, M.N. Tahir, M. Iqbal, K.S. Munawar. *J. Coord. Chem.*, **67**, 2479 (2014).
- [27] N. Ali, M.N. Tahir, S. Ali, M. Iqbal, K.S. Munawar, S. Perveen. *J. Coord. Chem.*, **67**, 1290 (2014).
- [28] V. Zelenák, Z. Vargová, K. Györyová. *Spectrochim. Acta, Part A*, **66**, 262 (2007).
- [29] Z. Rehman, S. Shahzadi, S. Ali, G.-X. Jin. *Turk. J. Chem.*, **31**, 435 (2007).
- [30] Z. Rehman, N. Muhammad, S. Ali, A. Meetsma. *Acta Crystallogr.*, **E63**, m89 (2007).
- [31] A. Shah, E. Nosheen, S. Munir, A. Badshah, R. Qureshi, Z. Rehman, N. Muhammad, H. Hussain. *J. Photochem. Photobiol., B*, **120**, 90 (2013).
- [32] S.S. Kalanur, U. Katrahalli, J. Seetharamappa. *J. Electroanal. Chem.*, **636**, 93 (2009).
- [33] I. Haq. *Arch. Biochem. Biophys.*, **403**, 1 (2002).
- [34] G. Barone, A. Terenzi, A. Lauria, A.M. Almerico, J.M. Leal, N. Busto, B. García. *Coord. Chem. Rev.*, **257**, 2848 (2013).
- [35] S. Anbu, M. Kandaswamy. *Polyhedron*, **30**, 123 (2011).
- [36] J. Lu, X. Liao, B. Wu, P. Zhao, J. Jiang, Y. Zhang. *J. Coord. Chem.*, **66**, 1574 (2013).
- [37] M.R. Malik, V. Vasylyeva, K. Merz, N. Metzler-Nolte, M. Saleem, S. Ali, A.A. Isab, K.S. Munawar, S. Ahmad. *Inorg. Chim. Acta*, **376**, 207 (2011).